

Title:

Prediction of atherosclerotic changes in cavernous carotid aneurysms based on computational fluid dynamics analysis: A proof-of-concept study

Authors: Shintaro Nakajima, MD,1,2 Shinichiro Sugiyama, MD,3 Hidenori Oishi, MD,2,4 Kenichi Sato, MD,1 Yasushi Matsumoto, MD,1 Kuniyasu Niizuma, MD,3,5,6 Miki Fujimura, MD,7 Teiji Tominaga, MD,3

Affiliations:

1 Department of Neuroendovascular Therapy, Kohnan Hospital, Sendai, Japan

2 Department of Neurosurgery, Juntendo University Faculty of Medicine, Tokyo, Japan

3 Department of Neurosurgery, Tohoku University Graduate School of Medicine, Sendai, Japan

4 Department of Neuroendovascular Therapy, Juntendo University Faculty of Medicine, Tokyo, Japan

5 Department of Neurosurgical Engineering and Translational Neuroscience, Graduate School of Biomedical Engineering, Tohoku University, Sendai, Japan

6 Department of Neurosurgical Engineering and Translational Neuroscience, Tohoku University Graduate School of Medicine, Sendai, Japan

7 Department of Neurosurgery, Kohnan Hospital, Sendai, Japan

Corresponding Author:

Shintaro Nakajima, MD

Department of Neurosurgery

Juntendo University Faculty of Medicine

2-1-1 Hongo, Bunkyo-ku, Tokyo 113-8421, Japan.

Phone: +81-33-813-3111

Fax: +81-33-813-3111

E-mail: snnakaji@juntendo.ac.jp

*** Funding**

No funding was received for this study.

*** Conflict of interest**

The authors declare that they have no conflict of interest.

*** Ethical approval**

All procedures performed in the studies involving human participants were in accordance with the ethical standards of the institutional and/or national research committee and with the 1964 Helsinki Declaration and its later amendments or comparable ethical standards.

*** Informed consent**

Informed consent was obtained from all individual participants included in the study.

*** Acknowledgments**

We thank Dr. Ayako Shimizu (Tohoku University), Dr. Teruyoshi Saijo (Kohnan Hospital), Dr. Tomohiro Chiba (Kohnan Hospital), and Dr. Koetsu Sato (Kohnan hospital) for their technical support. We also thank Editage (www.editage.jp) for the English language review.

Authors contribution list

Title: Prediction of atherosclerotic changes in cavernous carotid aneurysms based on computational fluid dynamics analysis: A proof-of-concept study

Conceptualization: Shintaro Nakajima, Shinichiro Sugiyama

Methodology: Shintaro Nakajima, Shinichiro Sugiyama, Kenichi Sato, Yasushi Matsumoto

Formal analysis and investigation: Shintaro Nakajima, Shinichiro Sugiyama

Writing-original draft preparation: Shintaro Nakajima, Shinichiro Sugiyama

Review and editing: Hidenori Oishi, Kuniyasu Niizuma, Miki Fujimura

Funding acquisition: Shinichiro Sugiyama, Hidenori Oishi, Kuniyasu Niizuma, Miki Fujimura

Resources: Shinichiro Sugiyama, Kuniyasu Niizuma, Teiji Tominaga

Supervision: Teiji Tominaga

1 **TITLE**

2 **Prediction of atherosclerotic changes in cavernous carotid aneurysms based on**
3 **computational fluid dynamics analysis: A proof-of-concept study**

4

5

6 **ABSTRACT**

7 **Purpose:** Recent computational fluid dynamics (CFD) studies have demonstrated the
8 concurrence of atherosclerotic changes in regions exposed to prolonged blood residence.
9 In this proof-of-concept study, we investigated a small but homogeneous cohort of large,
10 cavernous carotid aneurysms (CCAs) to establish the clinical feasibility of CFD analysis
11 in treatment planning, based on the association between pathophysiology and
12 hemodynamics.

13 **Methods:** This study included 15 patients with individual large CCAs. We identified
14 calcifications, which indicated atherosclerotic changes, using the masking data of digital
15 subtraction angiography. We conducted a CFD simulation under patient-specific inlet
16 flow rates measured using magnetic resonance (MR) velocimetry. In the post-CFD
17 analysis, we calculated the blood residence time (ξ) and segmented the surface exposed
18 to blood residence time over 1 second ($S_{\xi>1}$). We measured the decrease in volume after
19 flow diversion using the original time-of-flight MR angiography data.

20 **Results:** Calcifications were observed in the region with $S_{\xi>1}$. In addition, the ratio of
21 $S_{\xi>1}$ to the surface of the aneurysmal domain exhibited a negative relationship with the
22 rate of volume reduction at the 6- and 12-month follow-ups. Post-CFD visualization
23 demonstrated that intra-aneurysmal swirling flow prolonged blood residence time under
24 the condition of a small inlet flow rate, when compared to the aneurysmal volume.

1 **Conclusion:** The results of this study suggest the usefulness of CFD analysis for the
2 diagnosis of atherosclerotic changes in large CCAs that may affect the therapeutic
3 response after flow diversion.

4
5
6 **KEYWORDS:** aneurysm, blood residence time, computational fluid dynamics,
7 atherosclerosis, hemodynamics, flow diversion

10 **INTRODUCTION**

11 The hemodynamic characteristics of cerebral aneurysms are unique compared to those of
12 normal blood vessels. [1-4] The term aneurysm refers to a “pouch” arising from a vessel
13 tube in which unstable flow structures such as swirling or re-circulation can be observed.
14 [5, 6] Such structures are unusual in a circular tube. Previously, the hemodynamics
15 peculiar to cerebral aneurysms were too complex to study using existing medical
16 modalities. However, recent progress in computational fluid dynamics (CFD) technology
17 and rapid increases in computational power have enabled us to examine the
18 hemodynamics of cerebral aneurysms. [1, 7, 8]

19 CFD is one of the main branches of fluid mechanics. The fluid domain is divided
20 by fine grids on a computer, and the governing equations of the fluid are solved via large-
21 scale computational analysis. The primary results for velocity and pressure are provided
22 for any computational grid with sufficient spatial and temporal resolution. Using the
23 primary results of CFD, we can reproduce the flow field in the object domain as an “*in*
24 *silico*” computer simulation. In addition, we can calculate secondary parameters such as

1 wall shear stress in a post-CFD analysis to achieve various research purposes. [1, 7, 8]

2 The detailed blood flow information provided by CFD can provide new insight
3 into the correlation among hemodynamics, anatomical geometry, and the
4 pathophysiology of cerebral aneurysms. [9-11] Hemodynamic instability in cerebral
5 aneurysms is associated with anatomical geometry, including the morphology of the
6 aneurysmal sac and the configuration of the parent arteries. [2-4, 11, 12] Hemodynamic
7 instability also leads to inflammatory remodeling of the aneurysmal wall. [9] Destructive
8 remodeling results in the growth of the aneurysm, which in turn increases the instability
9 of intra-aneurysmal hemodynamics. [9-11] On the other hand, inflammation of the
10 aneurysmal wall also promotes atherosclerotic changes that may play a protective role in
11 the prevention of further growth or rupture. [6, 9, 13, 14]

12 In previous CFD studies, the authors proposed that blood residence time can be
13 used to quantify intra-aneurysmal hemodynamic instability. [6, 13] The residence time of
14 a fluid is a secondary parameter that is calculated from the primary results of CFD
15 analysis and is used as an index of fluid instability. [15] In a small cohort of unruptured
16 middle cerebral artery aneurysms, the authors reported that swirling flow or re-circulatory
17 flow prolonged blood residence time inside the aneurysm, and that the aneurysmal wall
18 exposed to such unstable flow experienced atherosclerotic changes. [6] The association
19 between flow instability and atherosclerosis is well known in large arteries. [16, 17]
20 Moreover, the most recent CFD research has confirmed its relevance in cerebral
21 aneurysms using a large multicenter database that contains aneurysms originating at
22 various locations. [14]

23 In the present proof-of-concept study, we investigated a small but homogeneous
24 cohort of large, cavernous carotid aneurysms (CCAs). Patients with CCAs were

1 significantly more likely to be in female, and large CCAs are therapeutic targets for flow
2 diversion. [18-20] In contrast to open surgery, neuro-endovascular treatments including
3 flow diversion do not reveal the pathologic status of the aneurysmal wall, which may
4 affect the treatment outcome. In this study, we proposed a modified CFD method for
5 predicting atherosclerotic changes in patients with large CCAs, which may be clinically
6 useful when planning for flow diversion treatment.

7

8 **METHODS**

9 *Patient selection*

10 We retrospectively reviewed the clinical and radiological data of patients who underwent
11 flow diversion treatment. The inclusion criteria of this study were as follows: (1) a large
12 CCA (> 10 [mm]) (2) treated with a single stent (and no coils), (3) an observation period
13 lasting 12 months after treatment, and (4) availability of three-dimensional (3D) rotational
14 angiography for CFD simulation. The study design was approved by the institutional
15 review board (#2021-1021-2).

16

17 *Flow Diversion*

18 Dual antiplatelet therapy (aspirin 100 mg/day and clopidogrel 75 mg/day) was initiated
19 from 5 days prior to the intervention onward. A platelet aggregation test was performed
20 to confirm an adequate antiplatelet effect. The procedure was performed under general
21 anesthesia and systemic heparinization. All patients were treated by a single stent (the
22 Pipeline Flex Embolization Device [Medtronic/Covidien, Irvine, CA, USA]). Following
23 stent deployment, a cone beam computed tomography was performed to assess any
24 potential stent malposition. The stent apposition was improved using balloon angioplasty

1 as needed. All patients were followed up with conventional angiography every 6 months
2 posttreatment.

3

4 ***Identification of calcification using angiographic data***

5 We used the 3D data acquired for masking in digital subtraction angiography (DSA), in
6 which not only the skull but also calcifications were depicted as high-density structures.

7 We segmented the calcified regions and created fusion images of the aneurysm in the
8 DSA images and calcified regions in the masking images.

9

10 ***Magnetic resonance velocimetry***

11 Phase-contrast (pc-) MR velocimetry is the standard method for measuring blood flow in
12 a human artery. [21] We measured blood flow rates at ipsilateral ICA prior to flow
13 diversion treatments by pc-MR velocimetry. Details of the pc-MR sequence are provided
14 in Online Resource 1.

15 The acquired phase-contrast images were transferred to a workstation for flow
16 quantification using dedicated software (CV Flow; GE Healthcare Japan, Tokyo, Japan).
17 [22] A region of interest was placed semi-automatically on phase-contrast images over a
18 cardiac cycle. The velocities at all pixels inside the vessel border were integrated to
19 calculate the flow in milliliters per second; these values were used to obtain the
20 quantitative waveform over the cardiac cycle. The mean blood flow rate (\bar{Q} [m³/s]) was
21 calculated from the obtained waveform.

22

23 ***Model construction***

24 The data set obtained from rotational angiography was exported to a personal computer

1 to reconstruct the geometric structure of the aneurysm using open-source imaging
2 software (Vascular Modeling Tool Kit; www.vmtk.org). The segmented 3D surface was
3 then processed using commercial software (3-matic version 10; Materialize, Leuven,
4 Belgium). We smoothed the fine irregularities and cleared the branches, including the
5 ophthalmic artery, posterior communicating artery, and anterior choroidal artery. We
6 defined the domain of an aneurysm as the segment extending from the proximal edge to
7 the distal edge of the aneurysm neck. We created entry and exit planes perpendicular to
8 the center line of the parent artery (Figure 1). We measured the volume (V [m^3]) and the
9 surface (S [m^2]) of the domain.

10

11 *Computational fluid dynamics*

12 During pre-processing for the CFD simulation, we created an inlet plane at the cervical
13 portion of the internal carotid artery (ICA) and an outlet plane at the top of the ICA on
14 the reconstructed 3D aneurysm model. Care was taken to ensure the proper ICA length
15 for the numerical simulation. The distal parent artery was extended to the normal direction
16 of the outlet plane, if needed. All models were meshed using commercial software (ICEM
17 CFD; ANSYS, Inc., Lebanon, New Hampshire, USA) to create tetrahedral meshes with
18 five layers of finer prism meshes in the boundary, resulting in approximately 1.5 million.
19 A finite-volume method package, ANSYS 14.5, (ANSYS, Inc.), was used to solve the
20 governing equations, which included the 3D Navier–Stokes equations and the equation
21 of continuity. Following the conventions for CFD in cerebral aneurysms, the blood was
22 treated as an incompressible Newtonian fluid (density: $1,050 \text{ kg/m}^3$; viscosity: 0.004
23 $\text{Pa}\cdot\text{s}$), vessel walls were assumed to be rigid, and no-slip boundary conditions were
24 applied at the walls. [23] The mean flow rate of the ipsilateral ICA, measured using phase-

1 contrast MR velocimetry, was prescribed at the inlet boundary. [24] The diffusion fluxes
2 in the direction normal to the inlet plane were assumed to be zero, and the normal
3 gradients were neglected. The static pressure at the outlet was set to zero Pascal. All
4 models had one inlet and one outlet; therefore, the differential pressure was calculated to
5 satisfy the boundary conditions.

6 7 ***Blood residence time***

8 Blood residence time is calculated as a secondary parameter from the primary velocity
9 fields obtained by CFD, and is used as an index of hemodynamic instability in cerebral
10 aneurysms [13, 15].

11 We applied the concept whereby residence time represents the amount of time
12 the fluid has been in (or resided within) the domain. [13, 15, 25] A more detailed
13 description of the theory is provided Online Resource 1. The residence time of the fluid
14 (ξ [s]) was calculated from the velocity field (\mathbf{u} [m/s]) obtained via CFD analysis.

$$\frac{\partial}{\partial t}\xi + \nabla \cdot (\mathbf{u}\xi) = 1 \quad (1)$$

15 We calculated the average value of the blood residence time in the aneurysm
16 domain ($\bar{\xi}$ [s]).

17 18 ***Segmentation of the surface with long blood residence***

19 We segmented the surface with a blood residence using a certain threshold. The threshold
20 value was defined as the mean value plus two times the standard deviation of the $\bar{\xi}$ in
21 the 15 included cases. We demarcated the boundary of the aneurysmal surface based on
22 the threshold ($S_{\xi > threshold}$ on the aneurysmal surface and $S_{\xi = threshold}$ in the entire
23 aneurysmal domain).

1 In addition, we calculated the ratio between the surface of $S_{\xi > threshold}$ and that
2 of the entire domain (S). Based on the principle of hemodynamic–pathologic association
3 in cerebral aneurysms, the ratio of $S_{\xi > threshold}/S$ reflects the extent of atherosclerotic
4 change over the aneurysmal domain.

6 ***Volume reduction after flow diversion***

7 Using the original data of gradient-echo time-of-flight MR angiography, we measured the
8 volumes of aneurysms at 1 day (V_{1d} [m³]), 6 months (V_{6m} [m³]), and 12 months (V_{12m}
9 [m³]) after flow diversion. The volume reduction rate was calculated as follows:

$$Volume\ reduction\ rate = \frac{V_{1d} - V_M}{V_{1d}} \times 100 [\%] \quad (2)$$

$(M = 6m\ or\ 12m)$

11 ***Ratio of blood flow rate to aneurysmal volume***

12 Dividing the domain volume (V [m³]) by the flow rate entering the domain (Q [m³/s]) is
13 a simple metric for estimating the average time (T [s]) that is required to exchange fluid
14 inside the domain of interest.

$$T = \frac{V}{Q} \quad (3)$$

16 ***Statistical analysis***

17 We used Mann–Whitney U-tests for parametric statistical analyses. Categorical variables
18 were analyzed using Fisher’s exact tests. We estimated the linear relationship between
19 continuous variables using Pearson’s correlation coefficients. Statistical significance was
20 set at $P < 0.05$. All statistical analyses were performed using EZR (Saitama Medical Center,
21 Jichi Medical University, Saitama, Japan, version 1.54), which is a graphical user

1 interface for R (The R Foundation for Statistical Computing, Vienna, Austria, version
2 4.0.3). [26] More precisely, it is a modified version of R commander (version 2.7-1) that
3 was designed to add statistical functions frequently used in biostatistics.

4 5 **RESULTS**

6 15 patients were included in the study. Their median age was 62.5 (interquartile range
7 [IQR]: 58.5–70.8) years, and 14 patients were female. The median aneurysm size was
8 14.3 [mm] (IQR: 12.8–16.8 [mm]). Among the 15 patients included in this study, we
9 observed calcified changes in the aneurysmal wall in 6 patients (40.0%) (Online resource
10 2).

11 In all 15 patients, the CFD simulation reproduced the swirling flow inside the
12 aneurysm which was also observed during conventional angiography (Online Resource
13 3).

14 15 ***Blood residence time and aneurysmal calcification***

16 The mean and SD values of $\bar{\xi}$ among the 15 cases were 0.46 s and 0.27 s, respectively.
17 Therefore, we defined the threshold value (the mean value plus 2SD) as 1.00 s for the
18 segmentation of the surface with long blood residence ($S_{\xi>1}$ and $S_{\xi=1}$).

19 In Figure 2, we present the segmentation results for $S_{\xi>1}$. Calcifications on the
20 aneurysmal wall were observed in cases with the $S_{\xi>1}/S$ ratio of approximately 0.38 or over.
21 In addition, calcifications were located in the region of the $S_{\xi>1}$. The $S_{\xi>1}$ region was
22 significantly wider in calcified aneurysms than in non-calcified aneurysms (Figure 3).

23 24 ***Blood residence time and aneurysmal volume reduction***

1 We calculated the ratio of $S_{\xi>1}/S$ to examine the extent of atherosclerotic change over
2 the aneurysmal domain. We observed a negative relationship between the $S_{\xi>1}/S$ ratio
3 and the volume reduction rate at 6 and 12 months after flow diversion. In particular,
4 patients with an $S_{\xi>1}/S$ ratio greater than 0.5 exhibited a remarkable delay in absorption
5 after flow diversion (Figure 4).

6

7 ***Blood residence time and occlusion status 12 months after flow diversion***

8 In the angiographic follow-up 12 months after flow diversion, 8 patients showed complete
9 occlusion of the treated aneurysm (the O’Kelly-Marotta (OKM) grading scale D), while
10 7 patients showed partial occlusion (OKM scale B; 3 patients, OKM scale C; 4 patients).
11 [27]

12 The $S_{\xi>1}/S$ ratio was significantly higher in incompletely occluded aneurysms
13 than in completely occluded aneurysms (median: 0.526 [IQR :0.4175–0.6285] vs.
14 median: 0.0995 [IQR: 0.0205–0.216], $P = 0.00124$).

15

16 ***Intra-aneurysmal hemodynamics and blood residence time***

17 To investigate the correlation between blood residence time and intra-aneurysmal
18 hemodynamics, we superimposed the surface of $S_{\xi=1}$ in the flow field visualized by
19 streamlines (Figure 5 and Online Resource 3 and 4).

20 In all 15 patients, we observed swirling flow inside the aneurysm which was also
21 observed during conventional angiography. We observed re-circulatory flow (secondary
22 vortex flow) in one patient. In patients 10–15, the slow swirling flow caused a remarkable
23 prolongation of the blood residence time. In typical cases, $S_{\xi=1}$ exhibits a conical shape
24 with a vertex in the exit direction.

1

2 ***Blood residence time and blood exchange time***

3 According to Eq. 3, we calculated the time required for blood exchange (T) by dividing
4 the domain volume (V) by the blood flow rate (Q).

5 The graphs in Figure 6 show the positive correlation between T and $S_{\xi>1}$
6 (Pearson's correlation coefficient: 0.916, 95% confidence interval (CI): 0.762–0.972,
7 $P<0.001$) as well as T and the $S_{\xi>1}/S$ ratio (Pearson's correlation coefficient: 0.734, 95%
8 CI: -0.356 – 0.906 , $P=0.00183$), which implies that T influences the velocity of intra-
9 aneurysmal swirling flow.

10

11 **DISCUSSION**

12 In this proof-of-concept study, we aimed to establish the feasibility of and rationale for
13 the clinical use of CFD analysis in treatment planning for patients with large CCAs. We
14 conducted a CFD simulation under patient-specific inlet conditions measured using
15 phase-contrast MR velocimetry. [22, 24] In the post-analysis, we calculated blood
16 residence time from the primary results of the CFD simulation, following which we
17 identified the region exposed to unstable blood flow by prolonged blood residence over
18 1.0 s ($S_{\xi>1}$). We observed that atherosclerotic changes indicated by calcifications
19 coincided with the region of $S_{\xi>1}$. Moreover, the ratio of $S_{\xi>1}$ to the surface of the
20 whole domain (S) exhibited a negative relationship with decreases in aneurysm volume
21 after flow diversion treatment. The results of this study suggest the usefulness of CFD
22 analysis for the diagnosis of atherosclerotic changes in large CCAs that may affect the
23 therapeutic response after flow diversion.

24

In this study, we proposed a feasible CFD method that considers applicability to

1 clinical practice. We performed a steady-state simulation in a Newtonian viscosity setting,
2 based on the results of previous studies regarding the detailed hemodynamics of cerebral
3 aneurysms in which pulsatile transient simulations were conducted, with or without a
4 non-Newtonian viscosity setting. [12, 13, 28] These previous studies provided us with
5 two insights that encouraged us to simplify our CFD method for clinical application. First,
6 the hemodynamics of a cerebral aneurysm are highly dependent on geometry, and basic
7 flow structures such as intra-aneurysmal swirl are preserved during cardiac cycles. [6, 12]
8 Second, it makes little difference whether Newtonian or non-Newtonian viscosity settings
9 are used to reproduce the basic flow fields. [13, 28] In fact, the present results indicate
10 that a steady-state simulation with Newtonian viscosity settings successfully reproduces
11 the intra-aneurysmal swirl which can be observed during conventional angiography
12 (Online Resource 3). This finding was validated by the concurrence of atherosclerotic
13 changes in the area exposed to prolonged blood residence that resulted from the swirling
14 flow. In addition, the use of steady-state simulation saved hours of calculation time. The
15 substitution of the Newtonian viscosity setting for the non-Newtonian setting addressed
16 the issue of large variations in non-Newtonian blood viscosity, a patient-related factor that
17 is generally unavailable in clinical situations.

18 The present CFD study provides fundamental knowledge concerning the
19 hemodynamics of CCAs. In the post-CFD visualization, we observed intra-aneurysmal
20 swirling, which was also observed during conventional angiography, in all 15 patients
21 (Online Resources 3 and 4). The flow speed of the swirl depends on the ratio of the blood
22 flow rate in the parent artery to the volume of the aneurysm. When the flow rate is low
23 compared to the aneurysmal volume, swirling flow will be slow, thereby remarkably
24 prolonging blood residence time.

1 Atherosclerotic changes are implied when the blood residence time used to
2 segment the surface exceeds a certain threshold. The negative correlation between the
3 $S_{\xi>1}/S$ ratio and the rate of volume reduction indicates the resistance of the
4 atherosclerotic aneurysmal sac against physiological absorption after flow diversion.
5 Recent studies have revealed hemodynamic–pathologic interactions in cerebral
6 aneurysms. [9-11] As the size of the aneurysm increases, the blood residence time
7 increases, and the hemodynamic environment inside aneurysms switches from a high-
8 flow condition to a low-flow condition, which modulates inflammatory remodeling of the
9 aneurysm wall. [9-11, 29] Inflammatory thickening or atherosclerotic changes in the
10 aneurysm wall occur in areas with long blood residence times. [6, 13, 14, 30] The thick
11 and/or calcified aneurysmal wall develops a vasa vasorum, which supplies the aneurysmal
12 wall itself. [31] Despite the existence of the vasa vasorum, the blood supply to the
13 aneurysmal wall can be removed via trapping surgery. [32] On the other hand, the vasa
14 vasorum blood supply along the arterial wall remains after endovascular treatments. [33-
15 35] We speculate that the viability of the atherosclerotic aneurysmal wall due to the
16 development of the vasa vasorum causes resistance to physiological absorption after flow
17 diversion. [35]

18

19 ***Limitations***

20 The persistence of aneurysms after flow diversion is a multifactorial phenomenon. [36-
21 41] In particular, factors influencing post-treatment hemodynamics inside aneurysms,
22 such as stent apposition along a parent artery, strongly affect the treatment outcome. [41]
23 This proof-of-concept study included a small cohort. The significance of this finding in
24 clinical situations must be investigated in further studies using a large cohort.

1 Patients with CCAs were significantly more likely to be in female [20]. In fact,
2 our series consisted of 14 female (93.3%) patients. It is of interest whether there are any
3 hemodynamic differences between the sexes. A previous study reported that there was no
4 difference in cerebral blood flow between the sexes [21]. However, it might be desirable
5 to use patient-specific blood flow rate and blood pressure as boundary conditions for CFD
6 simulation. In this study, the former was available but the latter unavailable. Nevertheless,
7 we are confident of the study results because blood residence time is a robust parameter
8 for pressure setting.

9 Our study also had some mathematical/computational limitations. The steady-
10 state simulation was performed under the mean blood flow rate without considering
11 hemodynamic changes during cardiac cycles, meaning that it only reproduced the
12 “average” flow fields. [42] Neglecting non-Newtonian blood viscosity and vessel wall
13 elasticity results in the underestimation of blood residence time at the boundary near the
14 vessel/aneurysm wall. [13, 28] In the calculation of blood residence time, the diffusion of
15 fluid was not considered. [15] Therefore, future studies should consider the interpretation
16 of blood residence time in regions of flow stasis where blood diffusion occurs.

1 FIGURE LEGENDS

2 **Fig. 1** Computational hemodynamic analysis of a large, cavernous carotid aneurysm

3 (a) Setting the domain of an aneurysm (translucent pink). We defined the domain of an
4 aneurysm as the segment extending from the proximal edge to the distal edge of the
5 aneurysmal neck. We created an entry plane (blue) and an exit plane (yellow)
6 perpendicular to the center line of a parent artery. (b) Streamlines colored according to
7 the magnitude of the flow velocity. One can observe swirling blood flow inside the
8 aneurysm. (c) Streamlines colored according to blood residence time (ξ [s]). Blood
9 residence time was set to zero at the entry plane. (d) A contour map of ξ on the
10 aneurysmal wall. (e) The surface segmented according to ξ over 1 second ($S_{\xi>1}$). (f)
11 Isosurface of ξ equivalent to 1 second ($S_{\xi=1}$). Streamlines colored by ξ are also shown.
12 Note that the swirling flow caused prolongation of ξ

13

14 **Fig. 2** Visualization of the surface with a blood residence time over 1 second ($S_{\xi>1}$) in
15 cavernous carotid aneurysms. The percentage of $S_{\xi>1}$ to the surface of the whole domain
16 (S) is presented at each case ($\frac{S_{\xi>1}}{S} \times 100$ [%]). In cases with calcified aneurysms (#10-15),
17 we also display the three-dimensional angiography in which calcifications are colored in
18 yellow on the translucent aneurysmal wall. One can observe the concurrence of
19 calcifications in the $S_{\xi>1}$ region.

20

21 **Fig. 3** Box-and-whisker plots showing surface differences in areas with blood residence
22 times over 1 second ($S_{\xi>1}$) between calcified and non-calcified aneurysms. (a)
23 Comparison of the area of $S_{\xi>1}$ in calcified and non-calcified aneurysms. (b)
24 Comparison of the ratio of $S_{\xi>1}$ to the surface of the whole domain (S) in calcified and

1 non-calcified aneurysms

2

3 **Fig. 4** Graphs showing the correlation between the rate of volume reduction and the
4 $S_{\xi>1}/S$ ratio. (A) 6-month follow-up. (B) 12-month follow-up. S : surface of the entire
5 domain; $S_{\xi>1}$: surface of the region with blood residence time over 1 s

6

7 **Fig. 5** Isosurface of blood residence time (ξ) equivalent to 1 second ($S_{\xi=1}$) in calcified
8 aneurysms (patient #10-15). Streamlines colored by ξ are also shown. In all 6 aneurysms,
9 swirling flow caused the prolongation of ξ . Re-circulatory flow is also seen in patient
10 #10 (black arrow).

11

12 **Fig. 6** Graphs showing the positive linear relationships between blood exchange time (T)
13 and $S_{\xi>1}$ and between T and the $S_{\xi>1}/S$ ratio. (A) Correlation between T and $S_{\xi>1}$. (B)
14 Correlation between T and the $S_{\xi>1}/S$ ratio. S : surface of the entire domain; $S_{\xi>1}$:
15 surface of the region with blood residence time over 1 s

16

17 REFERENCES

18

- 19 1. Steinman DA, Milner JS, Norley CJ, Lownie SP, Holdsworth DW (2003) Image-
20 based computational simulation of flow dynamics in a giant intracranial
21 aneurysm. AJNR Am J Neuroradiol 24:559-566.
- 22 2. Hassan T, Timofeev EV, Saito T, Shimizu H, Ezura M, Matsumoto Y, Takayama
23 K, Tominaga T, Takahashi A (2005) A proposed parent vessel geometry-based
24 categorization of saccular intracranial aneurysms: computational flow dynamics

- 1 analysis of the risk factors for lesion rupture. *J Neurosurg* 103:662-680.
- 2 3. Castro MA, Putman CM, Sheridan MJ, Cebal JR (2009) Hemodynamic patterns
3 of anterior communicating artery aneurysms: a possible association with rupture.
4 *AJNR Am J Neuroradiol* 30:297-302.
- 5 4. Tremmel M, Dhar S, Levy EI, Mocco J, Meng H (2009) Influence of intracranial
6 aneurysm-to-parent vessel size ratio on hemodynamics and implication for
7 rupture: results from a virtual experimental study. *Neurosurgery* 64:622-630;
8 discussion 630.
- 9 5. Ujiie H, Tamano Y, Sasaki K, Hori T (2001) Is the aspect ratio a reliable index for
10 predicting the rupture of a saccular aneurysm? *Neurosurgery* 48:495-502;
11 discussion 502-3.
- 12 6. Sugiyama S, Niizuma K, Nakayama T, Shimizu H, Endo H, Inoue T, Fujimura M,
13 Ohta M, Takahashi A, Tominaga T (2013) Relative residence time prolongation in
14 intracranial aneurysms: a possible association with atherosclerosis. *Neurosurgery*
15 73:767-776.
- 16 7. Shojima M, Oshima M, Takagi K, Torii R, Hayakawa M, Katada K, Morita A,
17 Kirino T (2004) Magnitude and role of wall shear stress on cerebral aneurysm:
18 computational fluid dynamic study of 20 middle cerebral artery aneurysms. *Stroke*
19 35:2500-2505.
- 20 8. Saqr KM, Rashad S, Tupin S, Niizuma K, Hassan T, Tominaga T, Ohta M (2020)
21 What does computational fluid dynamics tell us about intracranial aneurysms? A
22 meta-analysis and critical review. *J Cereb Blood Flow Metab* 40:1021-1039.
- 23 9. Meng H, Tutino VM, Xiang J, Siddiqui A (2014) High WSS or low WSS?
24 Complex interactions of hemodynamics with intracranial aneurysm initiation,

- 1 growth, and rupture: toward a unifying hypothesis. *AJNR Am J Neuroradiol*
2 35:1254-1262.
- 3 10. Frosen J, Cebal J, Robertson AM, Aoki T (2019) Flow-induced, inflammation-
4 mediated arterial wall remodeling in the formation and progression of intracranial
5 aneurysms. *Neurosurg Focus* 47:E21.
- 6 11. Salimi Ashkezari SF, Mut F, Chung BJ, Robertson AM, Frosen J, Cebal JR
7 (2021) Analysis of hemodynamic changes from aneurysm inception to large sizes.
8 *Int J Numer Method Biomed Eng* 37:e3415.
- 9 12. Sugiyama S, Niizuma K, Sato K, Rashad S, Kohama M, Endo H, Endo T,
10 Matsumoto Y, Ohta M, Tominaga T (2016) Blood Flow Into Basilar Tip
11 Aneurysms: A Predictor for Recanalization After Coil Embolization. *Stroke*
12 47:2541-2547.
- 13 13. Sugiyama SI, Endo H, Niizuma K, Endo T, Funamoto K, Ohta M, Tominaga T
14 (2016) Computational Hemodynamic Analysis for the Diagnosis of
15 Atherosclerotic Changes in Intracranial Aneurysms: A Proof-of-Concept Study
16 Using 3 Cases Harboring Atherosclerotic and Nonatherosclerotic Aneurysms
17 Simultaneously. *Comput Math Methods Med* 2016:2386031.
- 18 14. Cebal JR, Detmer F, Chung BJ, Choque-Velasquez J, Rezai B, Lehto H, Tulamo
19 R, Hernesniemi J, Niemela M, Yu A, Williamson R, Aziz K, Shakur S, Amin-
20 Hanjani S, Charbel F, Tobe Y, Robertson A, Frosen J (2019) Local Hemodynamic
21 Conditions Associated with Focal Changes in the Intracranial Aneurysm Wall.
22 *AJNR Am J Neuroradiol* 40:510-516.
- 23 15. Haines, R (1999) Using residence time for the extraction of recirculation regions.
24 In: 14th Computational Fluid Dynamics Conference, Norfolk, VA, USA, pp. 345–

- 1 354.
- 2 16. Himburg HA, Grzybowski DM, Hazel AL, LaMack JA, Li XM, Friedman MH
3 (2004) Spatial comparison between wall shear stress measures and porcine arterial
4 endothelial permeability. *Am J Physiol Heart Circ Physiol* 286:H1916-22.
- 5 17. Malek AM, Alper SL, Izumo S (1999) Hemodynamic shear stress and its role in
6 atherosclerosis. *JAMA* 282:2035-2042.
- 7 18. Giovanni V, Thomas J.S, Ahmad Z.A, Roanna V, Giuseppe L (2020)
8 Cavernous sinus aneurysms: risk of growth over time and risk factors. *J Neurosurg*
9 132:22-26
- 10 19. Tanweer O, Raz E, Brunswick A, Zumofen D, Shapiro M, Riina HA, Fouladvand
11 M, Becske T, Nelson PK (2014) Cavernous carotid aneurysms in the era of flow
12 diversion: a need to revisit treatment paradigms. *AJNR Am J Neuroradiol*
13 35:2334-2340.
- 14 20. Oishi H, Teranishi K, Yatomi K, Fujii T, Yamamoto M, Arai H (2018) Flow
15 Diverter Therapy Using a Pipeline Embolization Device for 100 Unruptured
16 Large and Giant Internal Carotid Artery Aneurysms in a Single Center in a
17 Japanese Population. *Neurol Med Chir (Tokyo)* 58:461-467.
- 18 21. Zhao M, Amin-Hanjani S, Ruland S, Curcio AP, Ostergren L, Charbel FT (2007)
19 Regional cerebral blood flow using quantitative MR angiography. *AJNR Am J*
20 *Neuroradiol* 28:1470-1473.
- 21 22. Sugiyama S, Meng H, Funamoto K, Inoue T, Fujimura M, Nakayama T,
22 Omodaka S, Shimizu H, Takahashi A, Tominaga T (2012) Hemodynamic analysis
23 of growing intracranial aneurysms arising from a posterior inferior cerebellar
24 artery. *World Neurosurg* 78:462-468.

- 1 23. Steinman DA, Vorp DA, Ethier CR (2003) Computational modeling of arterial
2 biomechanics: insights into pathogenesis and treatment of vascular disease. *J Vasc*
3 *Surg* 37:1118-1128.
- 4 24. Najafi M, Cancelliere NM, Brina O, Bouillot P, Vargas MI, Delattre BM, Pereira
5 VM, Steinman DA (2021) How patient-specific do internal carotid artery inflow
6 rates need to be for computational fluid dynamics of cerebral aneurysms? *J*
7 *Neurointerv Surg* 13:459-464.
- 8 25. Jongen T (2004) Extension of the age-of-fluid method to unsteady and closed-
9 flow systems. *AIChE Journal*, 2020-2037.
- 10 26. Kanda Y (2013) Investigation of the freely available easy-to-use software 'EZR'
11 for medical statistics. *Bone Marrow Transplant* 48:452-458.
- 12 27. O'Kelly CJ, Krings T, Fiorella D, Marotta TR (2010) A novel grading scale for the
13 angiographic assessment of intracranial aneurysms treated using flow diverting
14 stents. *Interv Neuroradiol* 16:133-137.
- 15 28. Xiang J, Tremmel M, Kolega J, Levy EI, Natarajan SK, Meng H (2012)
16 Newtonian viscosity model could overestimate wall shear stress in intracranial
17 aneurysm domes and underestimate rupture risk. *J Neurointerv Surg* 4:351-357.
- 18 29. Gade PS, Tulamo R, Lee KW, Mut F, Ollikainen E, Chuang CY, Jae Chung B,
19 Niemelä M, Rezai Jahromi B, Aziz K, Yu A, Charbel FT, Amin-Hanjani S,
20 Frosen J, Cebal JR, Robertson AM (2019) Calcification in Human Intracranial
21 Aneurysms Is Highly Prevalent and Displays Both Atherosclerotic and
22 Nonatherosclerotic Types. *Arterioscler Thromb Vasc Biol* 39:2157-2167.
- 23 30. Furukawa K, Ishida F, Tsuji M, Miura Y, Kishimoto T, Shiba M, Tanemura H,
24 Umeda Y, Sano T, Yasuda R, Shimosaka S, Suzuki H (2018) Hemodynamic

- 1 characteristics of hyperplastic remodeling lesions in cerebral aneurysms. PLoS
2 One 13:e0191287.
- 3 31. Atkinson JL, Okazaki H, Sundt TM Jr, Nichols DA, Rufenacht DA (1991)
4 Intracranial cerebrovascular vasa vasorum associated with atherosclerosis and
5 large thick-walled aneurysms. *Surg Neurol* 36:365-369.
- 6 32. Lawton MT, Hamilton MG, Morcos JJ, Spetzler RF (1996) Revascularization and
7 aneurysm surgery: current techniques, indications, and outcome. *Neurosurgery*
8 38:83-92; discussion 92-4.
- 9 33. Dehdashti AR, Thines L, Willinsky RA, Tymianski M (2009) Symptomatic
10 enlargement of an occluded giant carotido-ophthalmic aneurysm after
11 endovascular treatment: the vasa vasorum theory. *Acta Neurochir (Wien)*
12 151:1153-1158.
- 13 34. Iihara K, Murao K, Sakai N, Soeda A, Ishibashi-Ueda H, Yutani C, Yamada N,
14 Nagata I (2003) Continued growth of and increased symptoms from a thrombosed
15 giant aneurysm of the vertebral artery after complete endovascular occlusion and
16 trapping: the role of vasa vasorum. Case report. *J Neurosurg* 98:407-413.
- 17 35. Numagami Y, Ezura M, Takahashi A, Yoshimoto T (1999) Antegrade
18 recanalization of completely embolized internal carotid artery after treatment of a
19 giant intracavernous aneurysm: a case report. *Surg Neurol* 52:611-616.
- 20 36. Bonney PA, Connor M, Fujii T, Singh P, Koch MJ, Stapleton CJ, Mack WJ,
21 Walcott BP (2020) Failure of Flow Diverter Therapy: Predictors and Management
22 Strategies. *Neurosurgery* 86:S64-S73.
- 23 37. Maragkos GA, Ascanio LC, Salem MM, Gopakumar S, Gomez-Paz S, Enriquez-
24 Marulanda A, Jain A, Schirmer CM, Foreman PM, Griessenauer CJ, Kan P,

1 Ogilvy CS, Thomas AJ (2019) Predictive factors of incomplete aneurysm
2 occlusion after endovascular treatment with the Pipeline embolization device. *J*
3 *Neurosurg* 132(5):1598-1605.

4 38. Awad AW, Kilburg C, Karsy M, Couldwell WT, Taussky P (2019) Change in the
5 angle of the anterior genu is associated with occlusion rate after Pipeline flow
6 diversion. *J Neurosurg* 1-5.

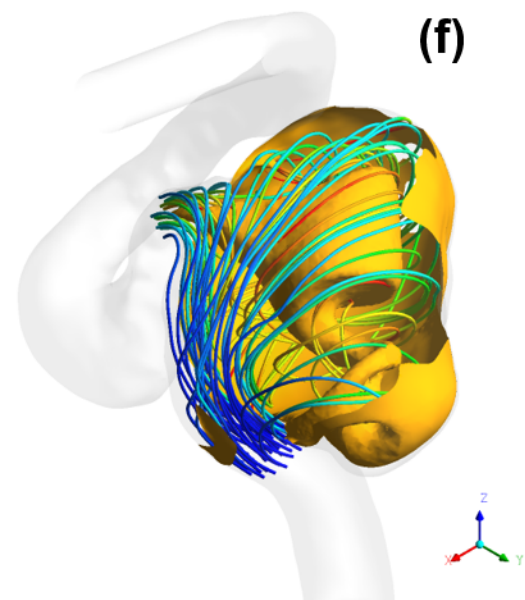
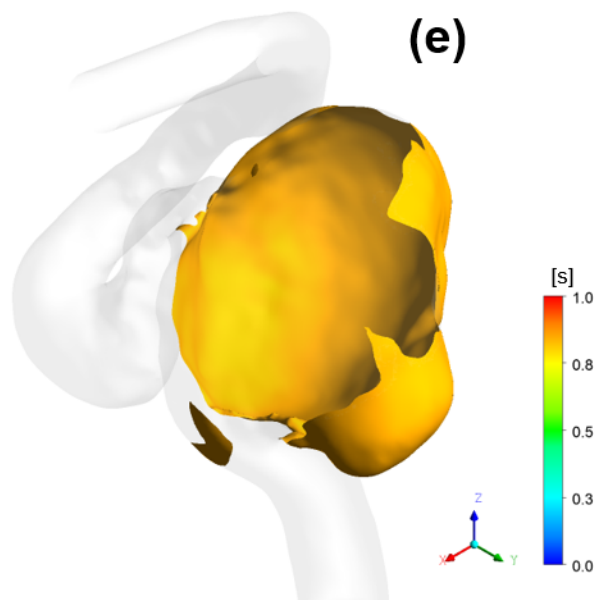
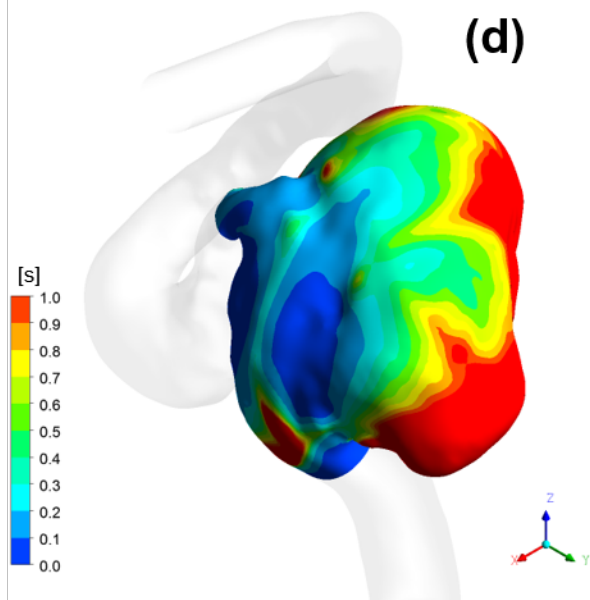
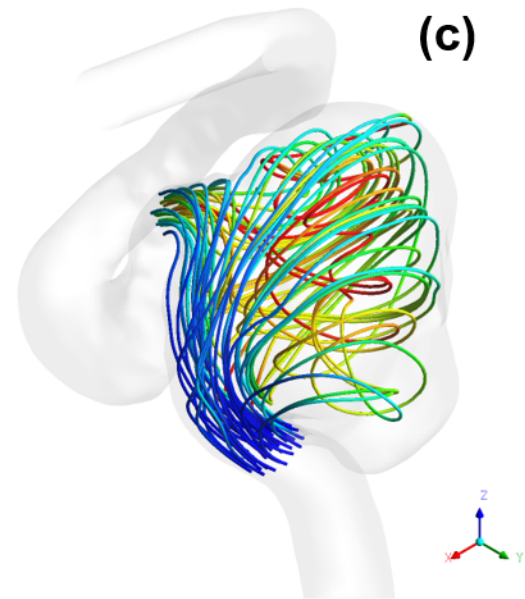
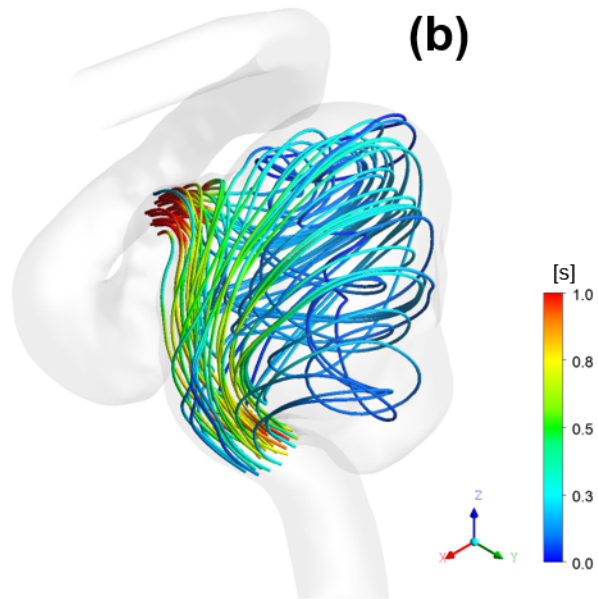
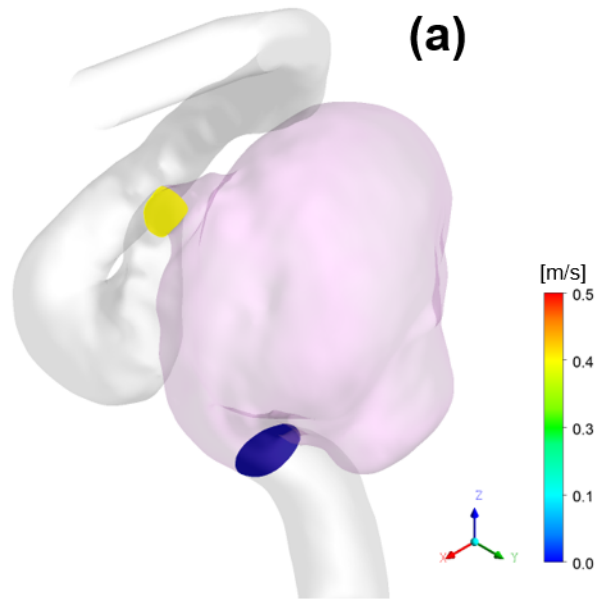
7 39. Trivelato FP, Salles Rezende MT, Ulhoa AC, Henrique de Castro-Afonso L,
8 Nakiri GS, Abud DG (2018) Occlusion rates of intracranial aneurysms treated
9 with the Pipeline embolization device: the role of branches arising from the sac. *J*
10 *Neurosurg* 1-7.

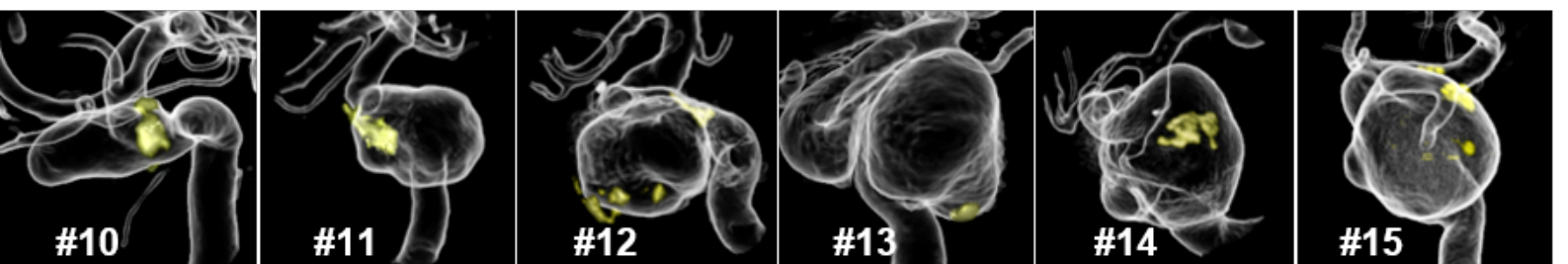
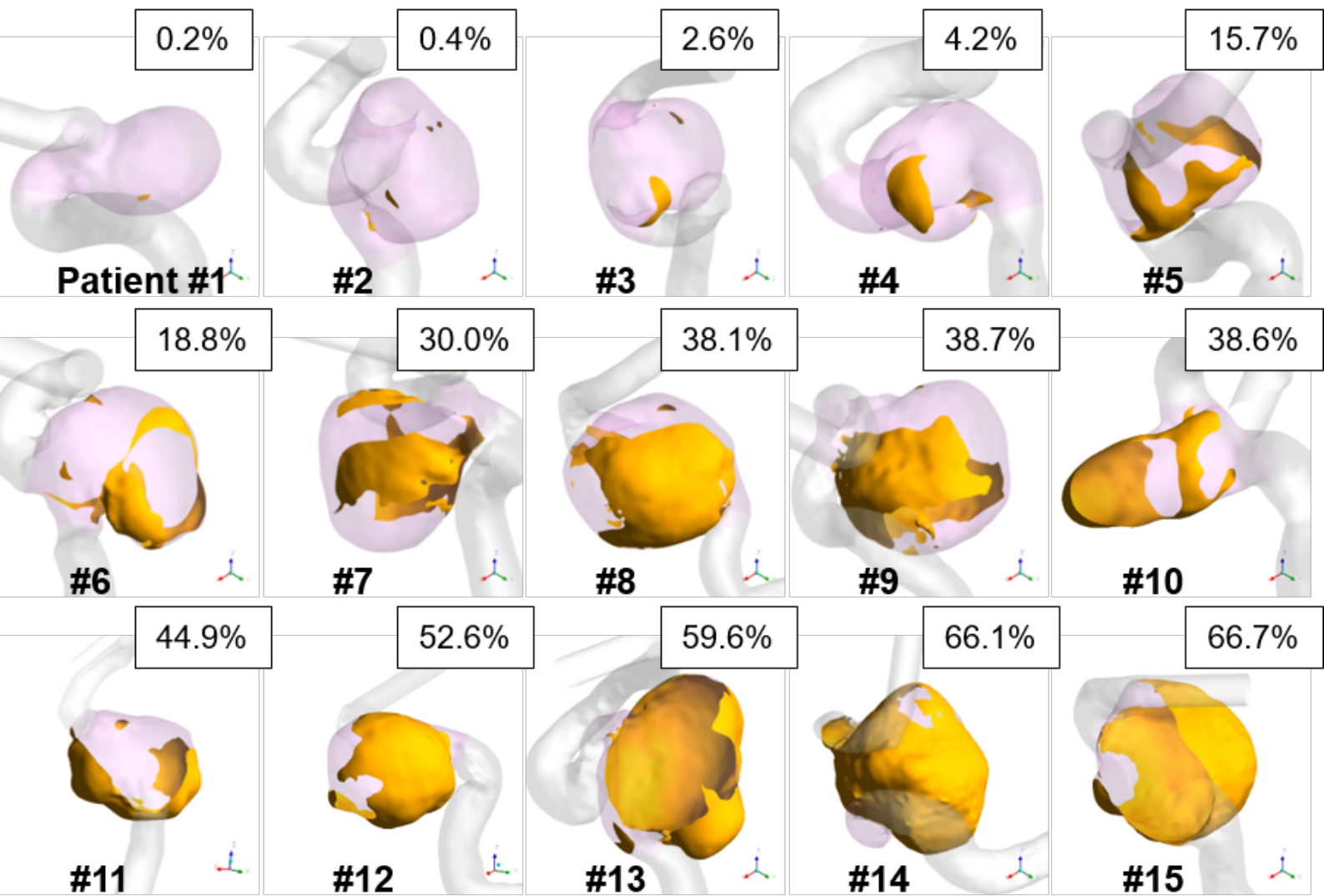
11 40. Paliwal N, Tutino VM, Shallwani H, Beecher JS, Damiano RJ, Shakir HJ, Atwal
12 GS, Fennell VS, Natarajan SK, Levy EI, Siddiqui AH, Davies JM, Meng H (2019)
13 Ostium Ratio and Neck Ratio Could Predict the Outcome of Sidewall Intracranial
14 Aneurysms Treated with Flow Diverters. *AJNR Am J Neuroradiol* 40:288-294.

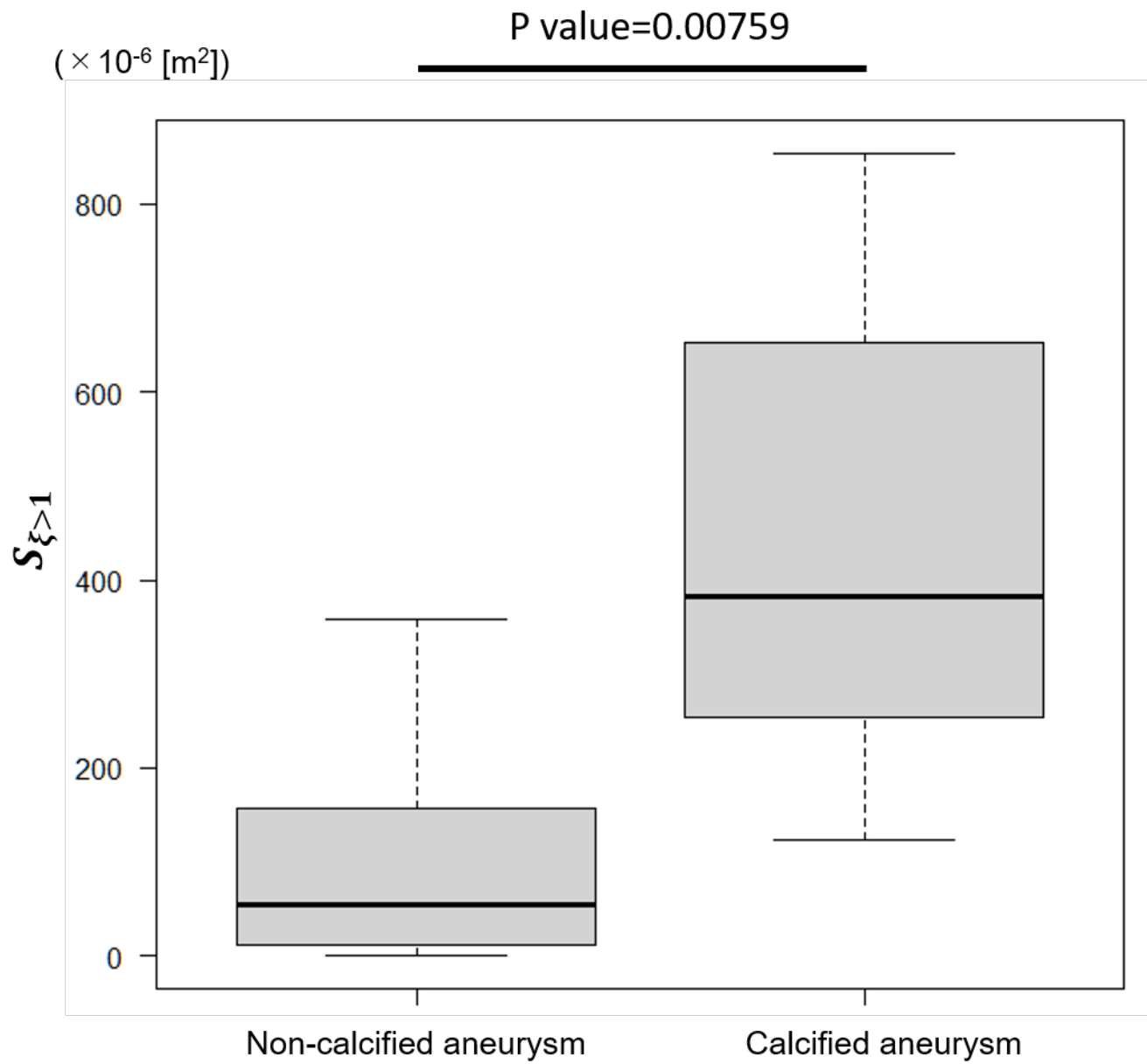
15 41. Rouchaud A, Ramana C, Brinjikji W, Ding YH, Dai D, Gunderson T, Cebra J,
16 Kallmes DF, Kadirvel R (2016) Wall Apposition Is a Key Factor for Aneurysm
17 Occlusion after Flow Diversion: A Histologic Evaluation in 41 Rabbits. *AJNR*
18 *Am J Neuroradiol* 37:2087-2091.

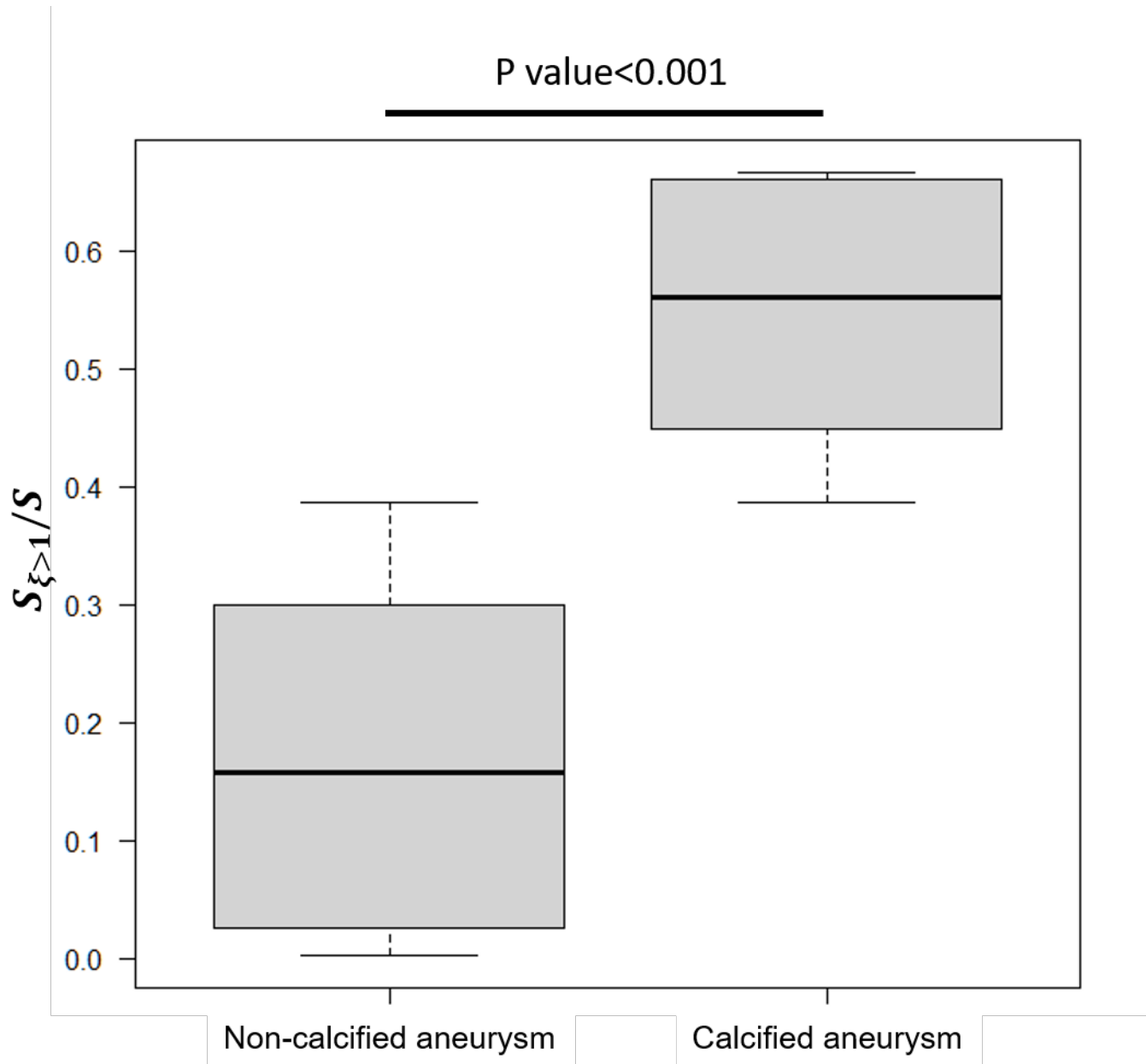
19 42. Geers AJ, Larrabide I, Morales HG, Frangi AF (2014) Approximating
20 hemodynamics of cerebral aneurysms with steady flow simulations. *J Biomech*
21 47:178-185.

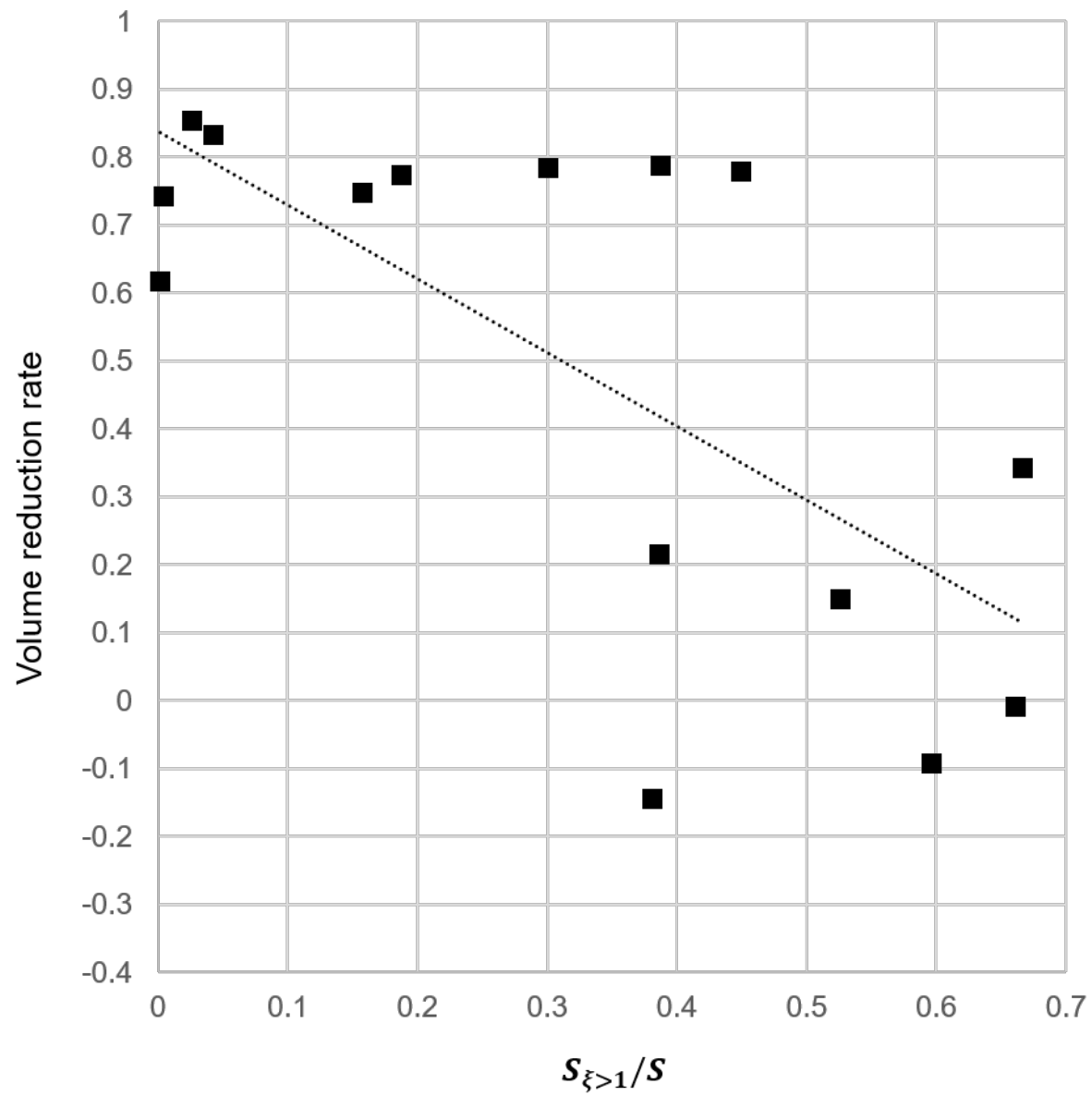
22
23

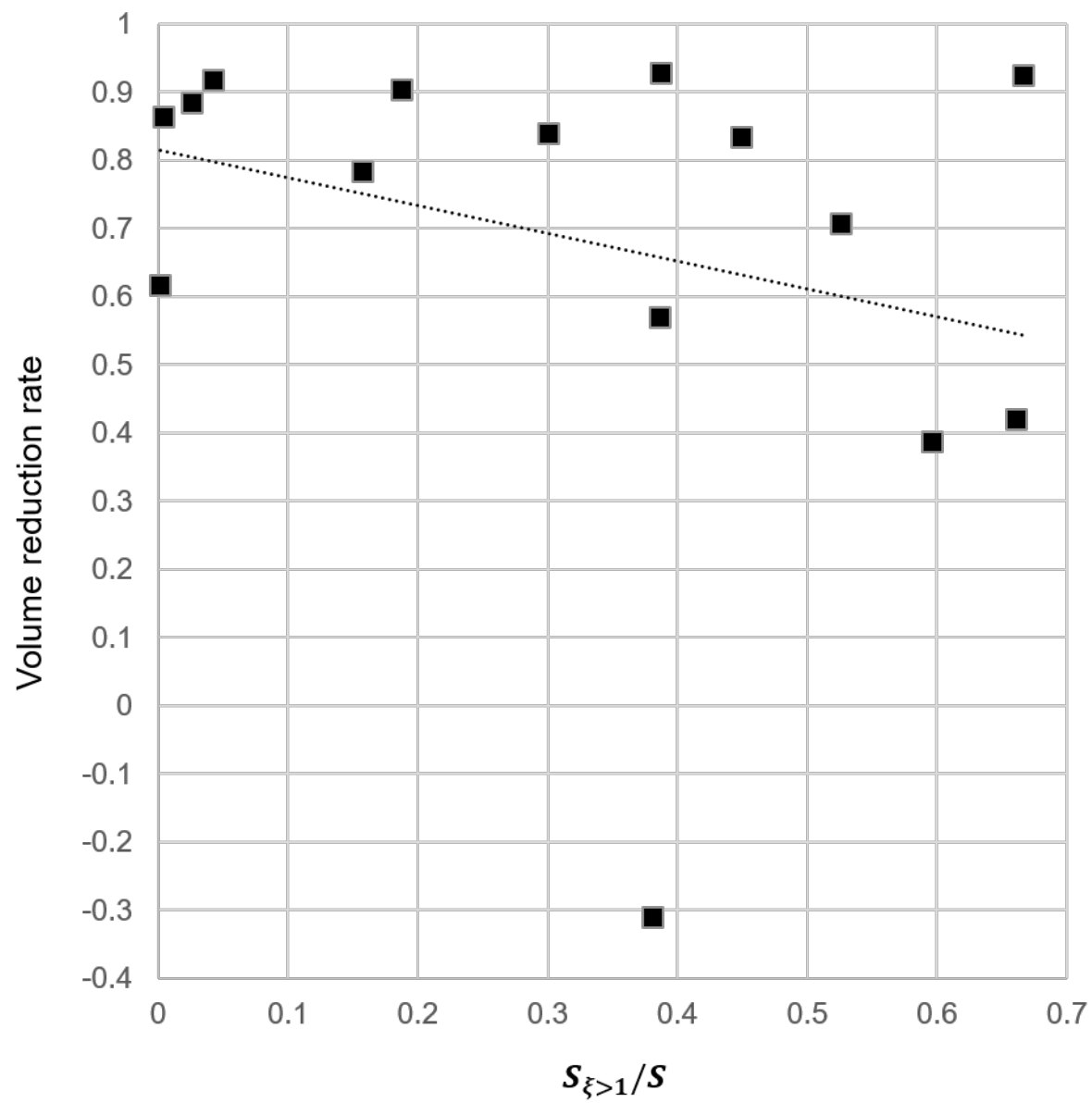




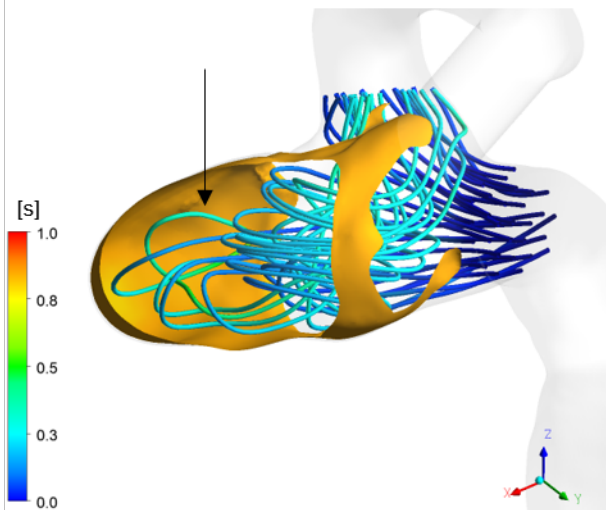




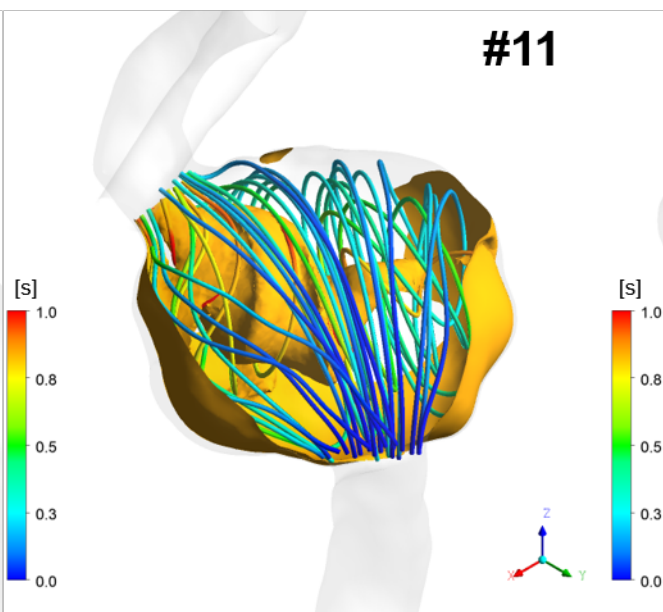




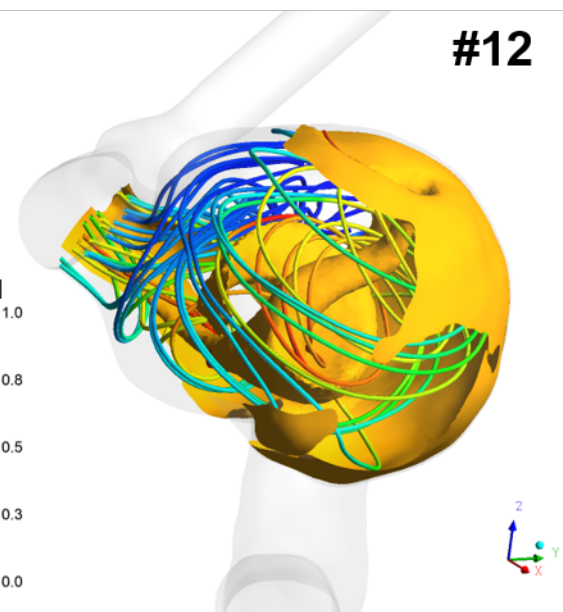
Patient #10



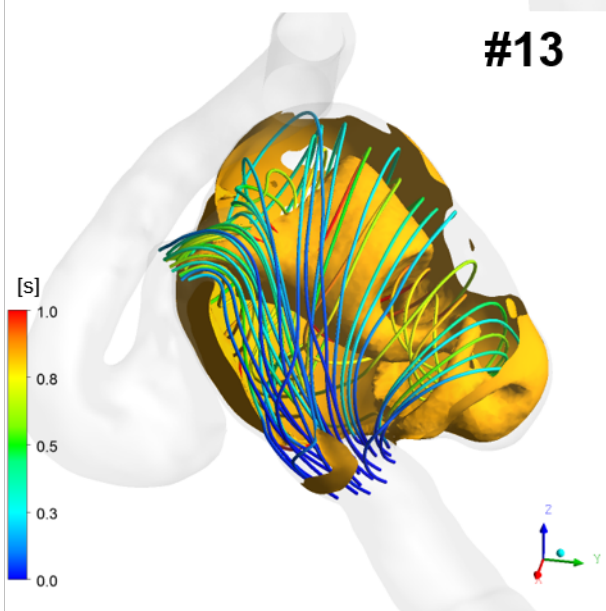
#11



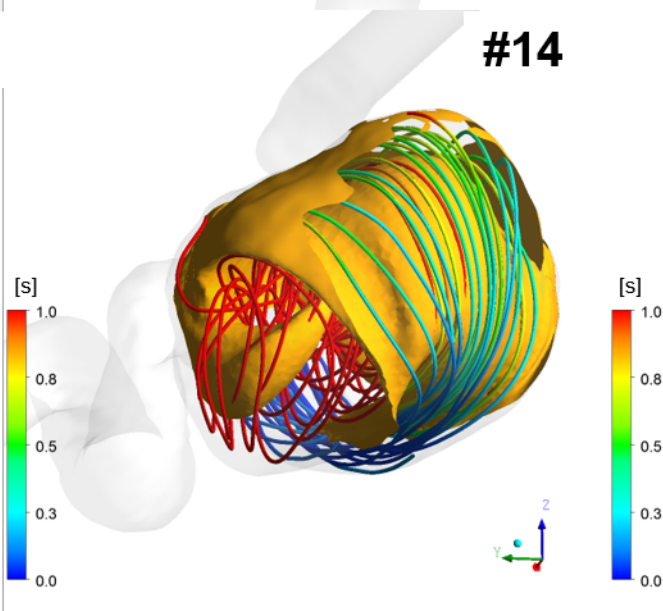
#12



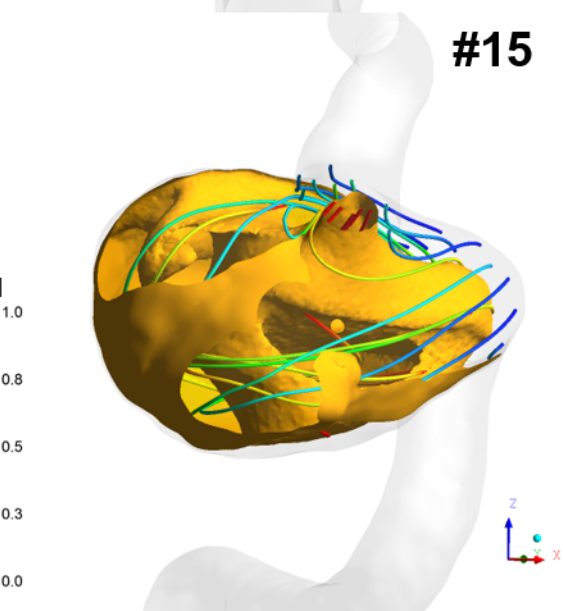
#13

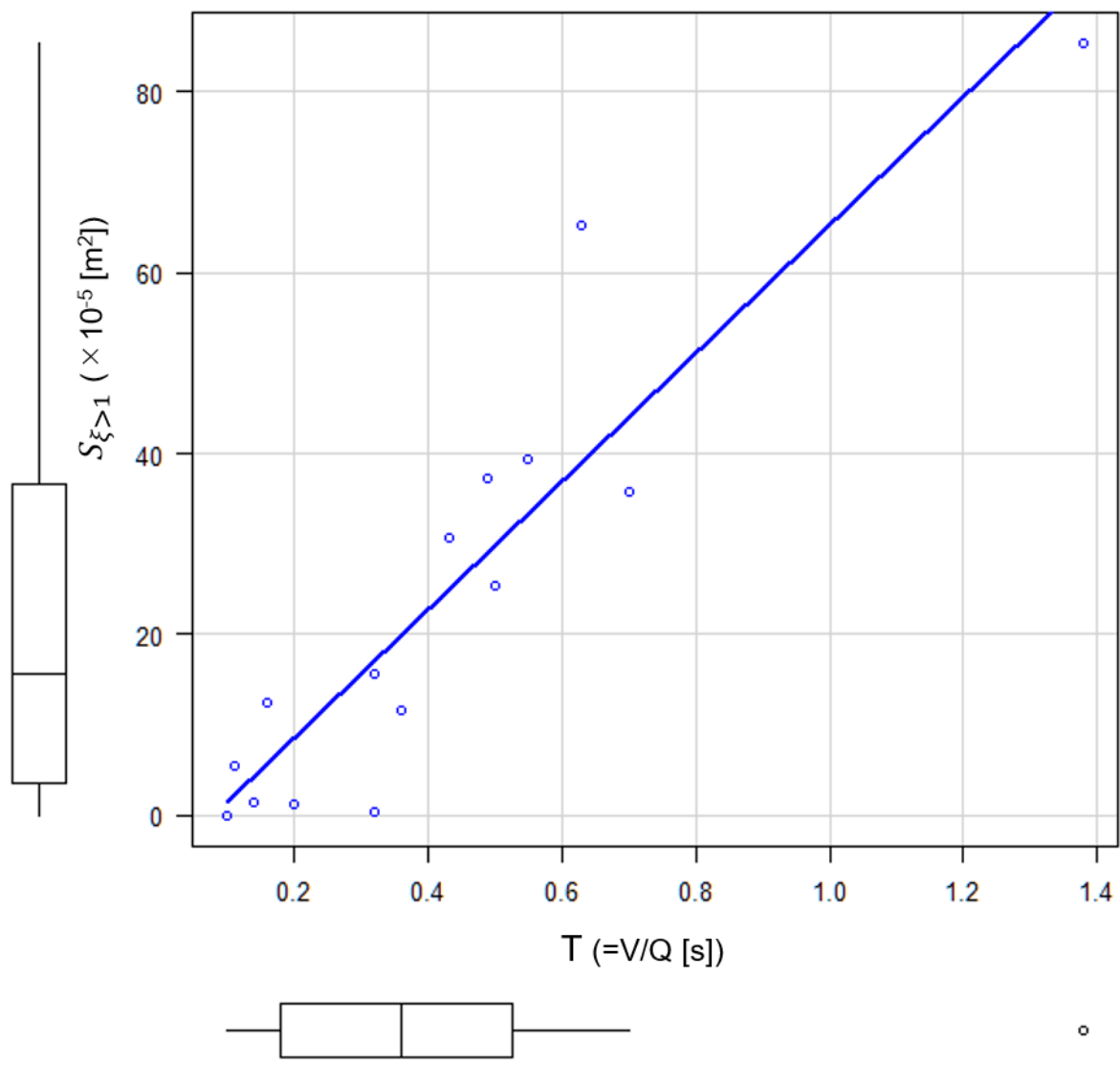


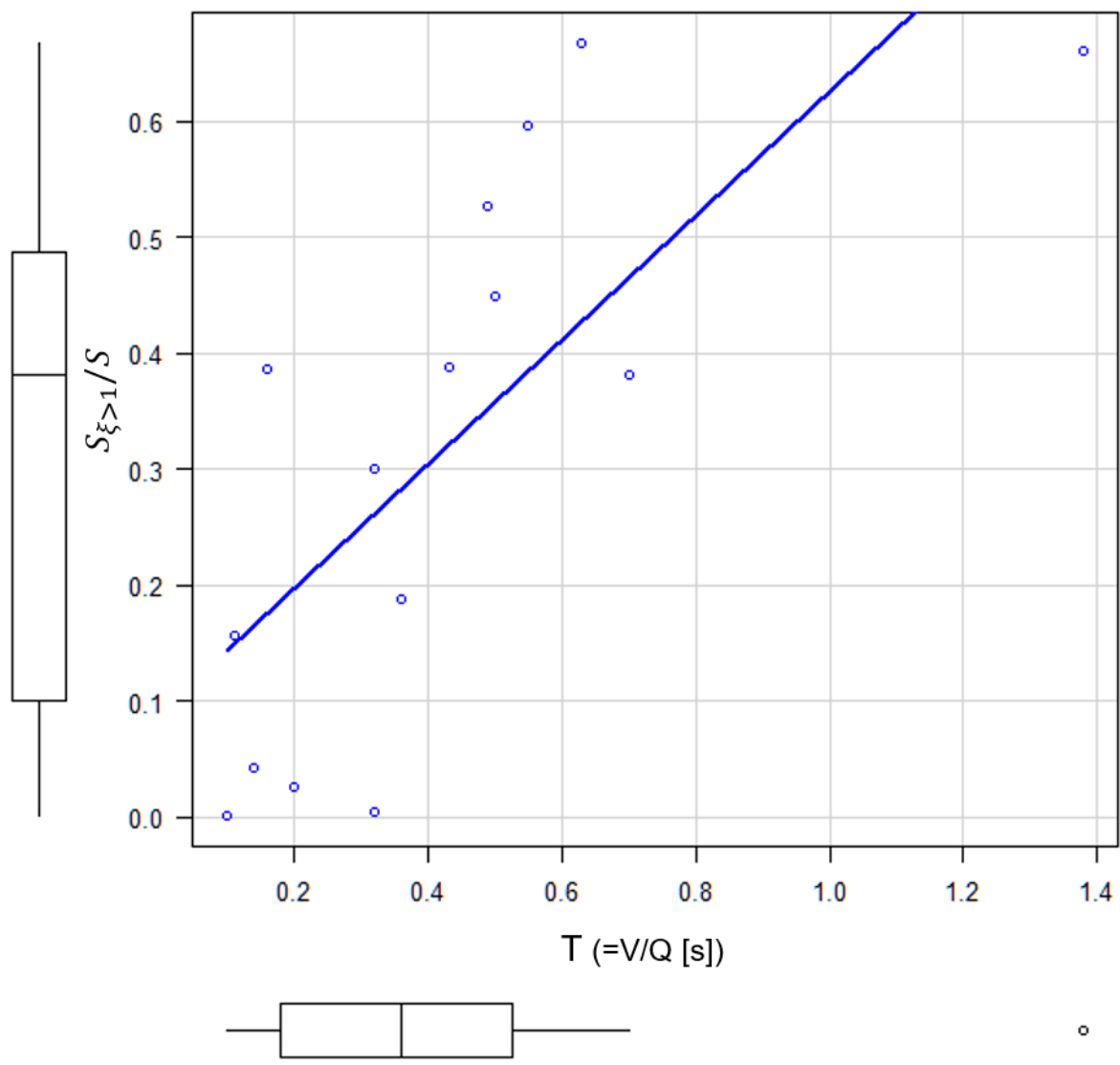
#14



#15







SUPPLEMENTAL METHODS

Magnetic resonance velocimetry

Quantitative magnetic resonance (MR) velocimetry was performed using a 3-T MR image scanner (Signa HDxt; GE Healthcare Japan, Tokyo, Japan) prior to flow diversion treatment. The protocol entails a standard cranial 3D time-of-flight MR angiography to select a slice orientation for arterial blood flow measurements. The optimal perpendicular scan plane was determined from the acquired time-of-flight (TOF) images at the C5 portion of an internal carotid artery. The coordinates obtained specified the position of an oblique fast two-dimensional (2D) phase-contrast sequence that was then performed on the basis of these coordinates using a peripheral gated 2D phase-contrast sequence. The imaging parameters were as follows: repetition time/echo time/number of excitations, 25 milliseconds/5.4 milliseconds/1; field of view, 160×160 mm; matrix, 512×512 ; voxel size, 0.3×0.3 mm; velocity encoding, 150 cm/s; imaging time, approximately 5 minutes; direction, transaxial; peripheral gated with ECG; and phases, 30.

Calculation of blood residence time

The residence time of the fluid was defined as the Eulerian transposition of the Lagrangian time. The residence time of a fluid parcel is the time elapsed since the parcel left the inlet in which its residence time is prescribed to be zero. When we consider a fluid parcel following a path described by its position vector $\mathbf{r}(t)$ at time t , $\mathbf{r}(t)$ is related to the velocity \mathbf{u} between two instants t_0 and t .

$$\mathbf{r}(t) = \mathbf{r}(t_0) + \int_{t_0}^t \mathbf{u}[s, \mathbf{r}(s)] ds \quad (1)$$

The residence time $\xi[t, \mathbf{r}(t)]$ of the fluid parcel at position \mathbf{r} at time t is given by

$$\xi[t, \mathbf{r}(t)] \equiv t - t_0 + \sigma[t_0, \mathbf{r}(t_0)] \quad (2)$$

We can assume that t_0 is the time when the fluid parcel left the inlet where the residence time is prescribed to be zero: $\xi[t_0, \mathbf{r}(t_0)] \equiv 0$. Therefore, we obtain the fundamental expression:

$$\mathbf{r}(t) - \mathbf{r}(t_0) = \int_{t-\xi[t, \mathbf{r}(t)]}^t \mathbf{u}[s, \mathbf{r}(s)] ds \quad (3)$$

which means that the residence time of a fluid parcel is the time elapsed along its path.

The derivative of Eq. 2 along the path and its Eulerian equivalent are as follows:

$$\frac{D}{Dt} \xi[t, \mathbf{r}(t)] = 1 \quad (4)$$

$$\frac{\partial}{\partial t} \xi + \nabla \cdot (\mathbf{u}\xi) = 1 \quad (5)$$

Supplemental table. Clinical and hemodynamic data of 15 cases

Case No.	Age/Sex	Surface with ζ over 1 second ($S_{\zeta>1}[\times 10^{-5} \text{ m}^2]$)	Proportion of $S_{\zeta>1}$ to S ($S_{\zeta>1}/S$)	Calcification (no=0, yes=1)
1	51/F	0.04	0.002	0
2	83/F	0.26	0.004	0
3	52/F	1.24	0.026	0
4	79/F	1.49	0.042	0
5	61/F	5.55	0.157	0
6	86/F	11.57	0.188	0
7	62/F	15.72	0.300	0
8	68/F	35.83	0.381	0
9	63/F	30.77	0.387	0
10	61/F	12.43	0.386	1
11	67/F	25.30	0.449	1
12	74/F	37.33	0.526	1
13	60/F	39.34	0.596	1
14	70/F	85.40	0.661	1
15	45/M	65.23	0.667	1